Title	Backward-angle photoproduction of ω and η' mesons from protons in the photon energy range from 1.5 to 3.0 GeV
Author(s)	Morino Yuhei, Hwang S., Imai Kenichi, Tanida Kiyoshi, LEPS Collaboration, 46 of others
Citation	Progress of Theoretical and Experimental Physics, 2015(1), p.013D01_1-013D01_11
Text Version	Publisher's Version
URL	https://jopss.jaea.go.jp/search/servlet/search?5053468
DOI	https://doi.org/10.1093/ptep/ptu167
Right	

PTEP

Prog. Theor. Exp. Phys. **2015**, 013D01 (11 pages)
DOI: 10.1093/ptep/ptu167

Backward-angle photoproduction of ω and η' mesons from protons in the photon energy range from 1.5 to 3.0 GeV

Y. Morino[1,2,*], Y. Nakatsugawa[3], M. Yosoi[1], M. Niiyama[4], M. Sumihama[19], T. Nakano[1], D. S. Ahn[2], J. K. Ahn[5], S. Ajimura[1], W. C. Chang[6], J. Y. Chen[1], S. Daté[7], H. Fujimura[8], S. Fukui[9], K. Hicks[10], T. Hiraiwa[1], T. Hotta[1], S. H. Hwang[11], K. Imai[11], T. Ishikawa[12], Y. Kato[9], H. Kawai[13], M. J. Kim[14], H. Kohri[1], Y. Kon[1], P. J. Lin[6], K. Mase[13], Y. Maeda[15], M. Miyabe[12], N. Muramatsu[12], H. Noumi[1], Y. Ohashi[7], T. Ohta[1], M. Oka[1], J. D. Parker[4], C. Rangacharyulus[16], S. Y. Ryu[1], T. Saito[13], T. Sawada[1], H. Shimizu[12], E. A. Strokovsky[17], Y. Sugaya[18], K. Suzuki[18], K. Tanida[15], A. Tokiyasu[1], T. Tomioka[13], T. Tsunemi[1], M. Uchida[20], R. Yamamura[1], and T. Yorita[1]

[1]*Research Center for Nuclear Physics, Osaka University, Ibaraki, Osaka 567-0047, Japan*
[2]*RIKEN Nishina Center for Accelerator-Based Science, Wako, Saitama 351-0198, Japan*
[3]*KEK, High Energy Accelerator Research Organization, Tsukuba, Ibaraki 305-0801, Japan*
[4]*Department of Physics, Kyoto University, Kyoto 606-8502, Japan*
[5]*Department of Physics, Korea University, Seoul 136-713, Korea*
[6]*Institute of Physics, Academia Sinica, Taipei 11529, Taiwan*
[7]*Japan Synchrotron Radiation Research Institute, Sayo, Hyogo 679-5143, Japan*
[8]*Wakayama Medical University, Wakayama 641-8509, Japan*
[9]*Department of Physics and Astrophysics, Nagoya University, Nagoya, Aichi 464-8602, Japan*
[10]*Department of Physics and Astronomy, Ohio University, Athens, OH 45701, USA*
[11]*Japan Atomic Energy Agency, Tokai-mura, Ibaraki 319-1195, Japan*
[12]*Research Center for Electron Photon Science, Tohoku University, Sendai, Miyagi 982-0826, Japan*
[13]*Department of Physics, Chiba University, Chiba 263-8522, Japan*
[14]*Department of Physics and Astronomy, Seoul National University, Seoul 151-747, Korea*
[15]*Proton Therapy Center, Fukui Prefectural Hospital, Fukui 910-8526, Japan*
[16]*Department of Physics and Engineering Physics, University of Saskatchewan, Saskatoon SK S7N 5E2, Canada*
[17]*Joint Institute for Nuclear Research, Laboratory of High Energy Physics, 141980, Dubna, Russia*
[18]*Department of Physics, Osaka University, Toyonaka, Osaka 560-0043, Japan*
[19]*Gifu University, Gifu 501-1193, Japan*
[20]*Department of Physics, Tokyo Institute of Technology, Tokyo 152-8551, Japan*
*E-mail: yuhei.morino@riken.jp

Received June 13, 2014; Accepted November 12, 2014; Published January 1, 2015

We report the measurement of differential cross sections for ω and η' photoproduction from protons at backward angles ($-1.0 < \cos\Theta^{X}_{C.M} < -0.8$) using linearly polarized photons at $E_\gamma = 1.5$–3.0 GeV. The differential cross sections for ω mesons are larger than the predicted u-channel contribution based on amplitude analysis in the energy range $2.0 \leq \sqrt{s} \leq 2.4$ GeV. The differential cross sections for ω and η' mesons become closer to the predicted u-channel contribution at $\sqrt{s} > 2.4$ GeV. A bump structure in the $\sqrt{s}$ dependence of the differential cross sections for η' mesons was observed at $\sqrt{s} \sim 2.35$ GeV.

Subject Index D24, D25

1. Introduction

Measurements of meson photoproduction provide a good tool to study nucleon resonances. Many nucleon resonances have been identified from experimental and theoretical studies of the πN scattering and π photoproduction. It is well known that a large number of missing resonances predicted by the constituent quark model remain to be discovered [1–3]. Some of the missing resonances may not be observed due to the weak coupling to the pion. However, there is a possibility of observing these missing resonances via the photoproduction of other strongly coupled mesons. Recently, the differential cross section and polarization variables of η, η', and ω mesons have been measured in experiments like CB-ELSA, GRAAL, and CLAS with large acceptance spectrometers [4–9]. Partial wave analysis (PWA) of their results indicates a significant contribution from nucleon resonances in the differential cross section of meson photoproduction at large scattering angles ($\Theta^X_{C.M} \sim \pi/2$) at $\sqrt{s} \sim 2$ GeV, although the list of resonances depends on the models.

At backward angles in the center-of-mass system, it is expected that the contribution from the u-channel exchange of Regge poles becomes significant. The differential cross section from the u-channel baryon exchange is expected to obey a power law behavior of s. In general, the differential cross section from the u-channel is much smaller than the one from the t-channel meson exchange. On the other hand, the angular distribution of mesons from nucleon resonances could have a rapid change at forward and backward angles when the nucleon resonances have high angular momenta. The contribution of nucleon resonances with high angular momenta tends to be stronger at forward and backward angles than at intermediate angles. Therefore, the differential cross section at backward angles is sensitive to nucleon resonances with high angular momenta and becomes a good tool to identify and search for these resonances. A bump structure in the s dependence of the differential cross section of η at very backward angles has been observed at SPring-8/LEPS [10].

A new measurement was carried out at SPring-8/LEPS with a time projection chamber (TPC) to detect decay products. In comparison with the previous LEPS experiment, background events of ω and η' signals were reduced substantially by using the TPC [10]. In addition, the incident photon energy, E_γ, was extended to 3.0 GeV by using a new deep-UV laser. In this paper, we report the differential cross sections of ω and η' photoproduction at backward angles ($-1.0 < \cos\Theta^X_{C.M} < -0.8$) from protons in the energy range $E_\gamma = 1.5$–3.0 GeV. The beam asymmetry is also reported for the ω photoproduction.

2. Experiment

The experiment was carried out at the SPring-8/LEPS facility [11]. A linearly polarized photon beam in the energy range from 1.5 to 3.0 GeV was produced by backward Compton scattering (BCS) from the head-on collision between laser photons and 8 GeV electrons in the storage ring. Both 355 nm and deep-UV 257 nm lasers were used to produce Compton-scattered photons in the range of 1.5 to 2.4 GeV and 1.5 to 3.0 GeV, respectively. The energy of a scattered photon was determined by measuring the recoil electron from Compton scattering by a tagging counter. The energy resolution for the photon beam was about 15 MeV. We used a liquid hydrogen (LH_2) target with a length of 15 cm and a diameter of 40 mm. The data were accumulated with 0.6×10^{12} photons from 1.5 to 2.4 GeV at the target with the 355 nm laser, and with 0.4×10^{12} photons from 1.5 to 3.0 GeV with the 257 nm laser, respectively [13]. Half of the data with the 355 nm laser (1.5–2.4 GeV) were taken with vertically polarized photons and the other half with horizontally polarized photons. The data with the 257 nm laser (1.5–3.0 GeV) were taken only with vertically polarized photons.

The LEPS forward spectrometer consisted of a dipole magnet, four multiwire drift chambers, a start counter (SC) just downstream of the target, a silica-aerogel Čerenkov counter (AC), and a time-of-flight (TOF) hodoscope placed downstream of the tracking detectors. In the measurement, one multiwire drift chamber was used instead of a silicon-strip vertex detector, unlike in the previous LEPS experiments. The angular coverage relative to the photon beam of the forward spectrometer was about ± 0.25 rad and ± 0.12 rad in the horizontal and vertical directions in the laboratory system, respectively. The TPC surrounding the target was installed inside a solenoid magnet. The main difference between the TPC and the one used in the previous LEPS experiment was the shape [12]. The TPC had a hexagonal hole in the center with a side length of 69 mm to install the LH_2 target. The TPC had an active volume of hexagonal cylinder shape with a side length of 225 mm and a height of 750 mm. The azimuthal and polar angular coverages of the TPC were 2π and 0.35–2.25 rad in the laboratory system, respectively. The TPC volume was filled with the P_{10} gas (Ar:CH_4 90%:10%). The signals from the TPC were read through rectangular cathode pads with a length of 56 mm and 150 mm. The typical spatial resolutions were 200–400 μm in the pad plane and 400–4000 μm in the beam direction depending on the direction of charged tracks. Six scintillation counters surrounded the target inside the TPC and twelve scintillation counters were placed outside of the TPC. We used a triple coincidence signal among the tagging counter and inner and outer counters as the trigger signal. This trigger signal corresponded to at least one charged particle track with $p_T \geq 0.09$ GeV/c in the TPC acceptance. The trigger efficiency saturated at about 94% in the geometrical acceptance of the scintillation counters.

3. Analysis

The photoproduction of the ω and η' mesons was measured via the following decay modes:

$$\gamma p \to p\omega \to p\pi^+\pi^-\pi^0 \quad (1)$$

$$\gamma p \to p\eta' \to p\pi^+\pi^-\eta. \quad (2)$$

Protons were measured by the LEPS forward spectrometer. Charged pions were detected in the TPC. π^0 or η mesons were identified by missing mass information to select the reactions (1) and (2). It was required that the number of reconstructed charged tracks in the TPC was one or two. The number of reconstructed electron tracks in the tagging counter was required to be one. Protons were selected by the mass reconstructed from momentum and TOF information within 4σ of the nominal value. The proton momentum was required to be more than 0.7 GeV/c because the ω and η' mesons were produced only in this range. Figure 1(a) shows the reconstructed mass square of positive charged particles as a function of momentum. Admixture of tracks from particles misidentified as protons was estimated to be negligible (<0.5%). The momentum resolution for protons was about 1%. Figure 1(b) shows the measured mean value of the energy deposition per pad (dE/dx) in the TPC of positive charged particles. The tracks with dE/dX below the threshold depending on their momentum were identified as pions. The dashed line in Fig. 1(b) shows the threshold line for pion identification with >98% efficiency. Although the cut for pion identification was not tight, tracks from particles misidentified as pions were suppressed since a proton was already detected in the forward spectrometer. The pions with $p_T \geq 0.08$ GeV/c were only reconstructed because of the center hole in the TPC. The momentum resolution for the pions was 4%–25%, strongly depending on momentum and polar angle of pions. A reaction point was determined as the intersection of a track reconstructed in the spectrometer and a track in the TPC. The spatial resolution of the reaction point

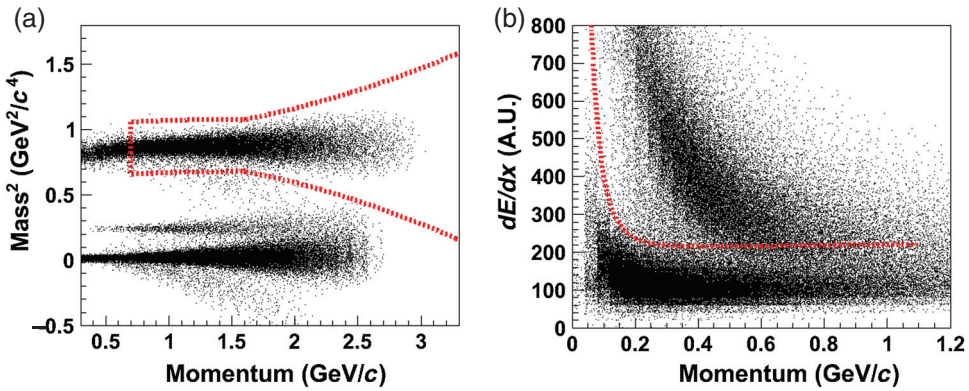

Fig. 1. (a) 2D scatter plot of mass squared and momentum of positive charged particles measured by the spectrometer. The dashed line shows the boundary for proton identification. (b) 2D scatter plot of the energy deposition and momentum for positive charged particles measured by the TPC. The dashed line shows the boundary for pion identification.

along the z direction was 2.6 mm. Events generated in the target were selected by the determined position of the reaction point. The effects of acceptance, efficiency, and resolution of the spectrometer and the TPC were evaluated using a Monte Carlo simulation with the GEANT3 code [14].

The systematic uncertainty in the cross section due to the target thickness including the target shape, fluctuations of the temperature, and pressure of the liquid hydrogen was estimated to be 2%. The systematic error of the photon number normalization was estimated to be 3% for data collected with the 355 nm laser and 4% for data with the 257 nm laser, respectively. This includes fluctuation of proton yield per photon and transmission ratio of the photon beam. The systematic error due to contamination from the events from the SC and the target cell was 1%. The systematic uncertainty due to the efficiency of proton detection was 4%, including geometrical acceptance (3%), wire efficiency (1%), and proton identification efficiency (2%). The systematic uncertainty due to the pion detection was 4%.

Figure 2(a) shows a missing mass spectrum for the $\gamma p \to pX$ reaction ($MM(p)$), where the photon energy is from 2.125 to 2.375 GeV and the scattering angle of protons is $0.90 < \cos\Theta^{P}_{C.M} < 1.00$. The spectra of missing mass squared for the $\gamma p \to p\pi^{\pm}X$ and $\gamma p \to p\pi^{+}\pi^{-}X$ reactions ($MM^2(p,\pi^{\pm})$ and $MM^2(p,\pi^{+},\pi^{-})$) are also shown in Figs. 2(e) and (f), respectively. Since the trigger requires at least one charged particle in the TPC acceptance, the peaks of η and π^0 mesons are not observed in Fig. 2(a), unlike the previous measurement [10]. The amount and/or the spectrum shape of other components are also modified due to the trigger in comparison with the previous measurement. Although the peak of the ω mesons overlaps with that of the ρ mesons, the ω signals can be separated from the ρ signals by identification of the decay products. To select the ω and η' signals, selection cuts were applied by using $MM^2(p,\pi^{\pm})$ and $MM^2(p,\pi^{+},\pi^{-})$. Figures 2(b) and (c) show the $MM(p)$ distribution with the ω and η' selection cuts, respectively. The details of the ω and η' selection cuts are summarized in Table 1. Figure 2(d) shows the $MM(p)$ distribution with an inverse η' selection cut. In the inverse η' selection cut, $MM^2(p,\pi^{+},\pi^{-})$ is used to reject the η' signal. This plot was prepared for the demonstration of understanding of the background shape.

We used the ω and η' selection cut for the evaluation of yields of the ω and η' mesons. Background for the ω and η' signals consisted of several reactions. To evaluate these contributions, possible reactions contributing to the $MM(p)$ distribution were generated in an event generator. The missing mass distributions of these reactions were determined by using Monte Carlo simulation. The relative yield

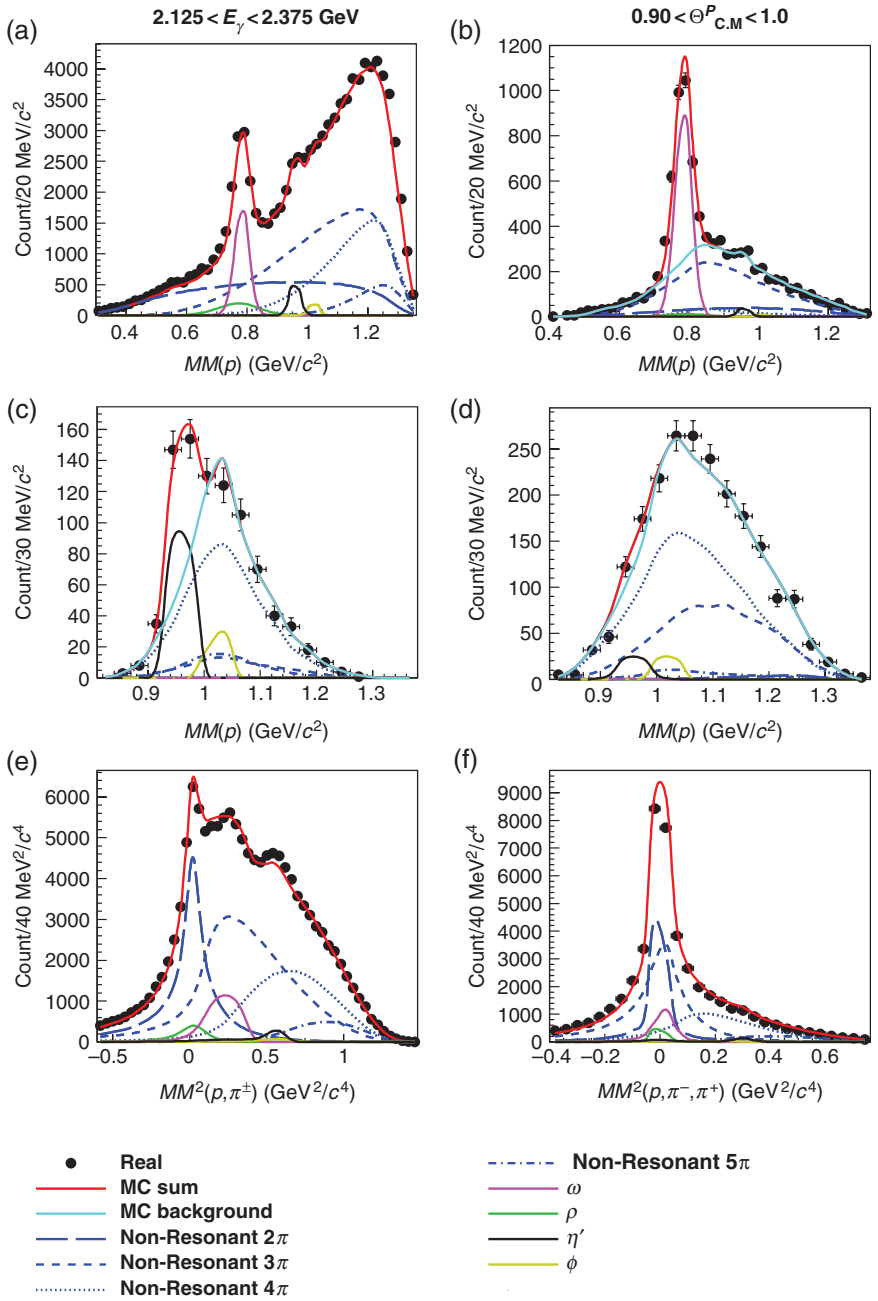

Fig. 2. Missing mass spectra for events with $2.125 < E_\gamma < 2.375$ GeV and $0.90 < \cos\Theta^P_{C.M} < 1.0$. The circles represent the experimental result. The red solid lines represent the sum of all contributions. The light blue lines represent the sum of the contributions without ω and η' contributions for panels (b) and (c), respectively. The blue dashed, dashed spaced, dotted, and chain lines represent non-resonant 2, 3, 4, and 5 π production, respectively. The magenta, green, black, and yellow lines represent ω, ρ, η', and ϕ, respectively. (a) $MM(p)$. (b) $MM(p)$ with the ω selection cut. (c) $MM(p)$ with the η' selection cut. (d) $MM(p)$ with the inverse η' selection cut. (e) $MM^2(p,\pi^\pm X)$. (f) $MM^2(p,\pi^+,\pi^-)$. C.M; Cener of Mass, MC; Monte-Carlo.

of each reaction was deduced by minimizing the χ^2 between the superposition of the determined distributions and the experimental data (a template fit). Events including non-resonant pions (from 2 to 5) and one proton were generated in the free N-body space as background components. Photoproductions of η, η', ρ, ω, and ϕ mesons were also generated as known resonances. The intrinsic width

Table 1. Summary of the ω, the η', and the inverse η' cut.

Cut (GeV$^2/c^4$)	$MM^2(p,\pi^\pm)$	$MM^2(p,\pi^+,\pi^-)$
ω	$0.05 < X < 0.44$	$-0.15 < X < 0.19$
η'	$0.40 < X < 0.72$	$0.24 < X < 0.36$
inverse η'	$0.40 < X < 0.72$	$0.10 < X < 0.24, 0.36 < X < 0.50$

of each meson was given according to the PDG [1]. The missing mass distribution of each meson was obtained by applying the GEANT3 simulation for the generated meson. Since the contribution from $K^0\Sigma^+$ photoproduction is negligible, it was not included. The distributions of $MM(p)$, $MM^2(p,\pi^\pm)$, $MM^2(p,\pi^+,\pi^-)$, and $MM(p)$ with a loose ω selection cut ($0.1 < MM^2(p,\pi^\pm) < 0.4\,\mathrm{GeV}^2/c^4$) were used as the constraint of the template fit simultaneously. While the amount of ρ is important for signal counting of ω, the separation of ρ and ω is difficult in the $MM(p)$ and $MM^2(p,\pi^+,\pi^-)$ distributions. The loose ω selection cut was applied to identify the ω peak. The distribution of $MM(p)$ with the loose ω selection cut was included in the fit to avoid the ρ/ω ambiguity. Events were put in photon energy bins with an interval of 62.5 MeV and proton scattering angle bins with a $0.05\cos\Theta^P_{C.M}$ interval. The template fit was performed for each bin on the photon energy and on the proton scattering angle. The reduced χ^2 was 0.9 at minimum and 2.9 at maximum, depending on the angular and energy bins. The contribution of each reaction in the fitting is shown in Figs. 2(a), (e), and (f), where the red solid lines represent the sum of all contributions and should be compared with the experimental results.

The $MM(p)$ distributions with the ω and η' selection cuts in each reaction were superposed according to the relative yields in the fitting result. The background shapes in the $MM(p)$ distributions with the selection cuts were determined as the superposition except the resonances corresponding to the selection cuts (ω or η'). The background shapes were normalized by template fits with the background and signal shapes of the $MM(p)$ distributions with the selection cuts. The determined background and the contribution of each component are shown in Figs. 2(b), (c), and (d). In Figs. 2(b), (c), and (d), the light blue solid lines represent the determined background and the red solid lines represent the sum of all contributions. The sum of all contributions reproduces the experimental results successfully, including the result with the inverse cut (Fig. 2(d)). The yields of the ω and η' signals were extracted by subtraction of the background. The yields were corrected by the number of photons, the number of target protons, and the efficiency of determining differential cross sections. The efficiency includes the branching ratios, the trigger efficiency, the efficiency of the event selection, the acceptance and efficiency of pions, the acceptance and efficiency of protons, and the efficiency of the selection cuts. The typical efficiency of the ω mesons was 23% at $-1.00 < \cos\Theta^\omega_{C.M} < -0.95$ and 9% at $-0.85 < \cos\Theta^\omega_{C.M} < -0.80$, respectively. The typical efficiency of the η' mesons was 6% at $-1.00 < \cos\Theta^{\eta'}_{C.M} < -0.80$.

The systematic uncertainty due to the trigger efficiency was 5%, including the uncertainty caused by the acceptance of the trigger counters (4%) and the uncertainty of the efficiency within the acceptance (3%). The systematic uncertainty due to the efficiency of the ω and η' selection cuts was estimated from the effect of varying the cut boundary and applying loose selection cuts. It was determined to be 3%. The systematic uncertainty due to the background shapes was estimated from the effect of varying the fit conditions (without the 5π reaction, reducing the fit constraint, the strategy of minimizing χ^2, and a combination of these). It was determined to be 3% and 5% for ω and η', respectively. Since there were only vertical polarization data in $E_\gamma = 2.4$–3.0 GeV,

the effect of polarization on the efficiency was included in the systematic uncertainty for this energy range. The effect on the efficiency was evaluated by Monte Carlo simulation as a function of beam asymmetry. The beam asymmetry in $E_\gamma = 2.4$–$3.0\,\mathrm{GeV}$ was assumed be less than 0.2. The systematic error due to the effect of polarization was 2–7% depending on the scattering angles.

4. Results and discussion

Figure 3 shows the differential cross sections for ω production as a function of $\sqrt{s}$. Each panel shows the result at the ω scattering angle regions ((a)–(d)) and the u interval ((e) and (f)). In $-0.9 < \cos\Theta^{\omega}_{C.M} < -0.8$, the results of CLAS are consistent with the present result, although the results of SAPHIR and CLAS are not consistent with each other [4,15]. The previous results of LEPS are also consistent with the present result [10]. The differential cross section decreases as $\sqrt{s}$ increases above $\sqrt{s} \sim 2.3\,\mathrm{GeV}$ in all the scattering angle bins. The dashed lines in Figs. 3(e) and (f) represent the result of a power law fit for the Daresbury results [17]. The smooth lines in Fig. 3 represent theoretical calculations, which do not include the s-channel contribution of nucleon resonances [19]. This calculation is based on the meson exchange model and considers the π, η, σ, and nucleon exchanges. A phenomenological form factor at the ωNN vertex was also introduced. The parameters in these calculations (coupling constants and cut-off parameters) were tuned to reproduce the Daresbury result, which had a kinematic range of $E_\gamma = 2.8$–$4.8\,\mathrm{GeV}$ and backward and forward scattering. It almost reproduces the Daresbury results, except the very steep s^{-8} dependence at $-0.2 < u < -0.1\,\mathrm{GeV}^2$. Since the ω production in the kinematic range of the Daresbury results is governed by the u-channel process, the extrapolation of the calculation to the LEPS energy range could be interpreted as the u-channel contribution.

The LEPS result shows that the present $\sqrt{s}$ dependence of $d\sigma/d\Omega$ is different from the theoretical calculation and the power law behavior for $\sqrt{s} \leq 2.4\,\mathrm{GeV}$. This implies that the present $\sqrt{s}$ dependence is difficult to explain by only the u-channel process, and that there is a significant s-channel contribution from nucleon resonances in this energy range. The LEPS and Daresbury results start showing power law behavior in $\sqrt{s} \geq 2.4\,\mathrm{GeV}$, which is expected in the u-channel process. To identify the possible nucleon resonances involved, we made a comparison between the present results and the theoretical calculation. The present results show a broad excess of $d\sigma/d\Omega$ at $2 \leq \sqrt{s} \leq 2.4\,\mathrm{GeV}$ compared with the theoretical calculation at $-0.95 < \cos\Theta^{\omega}_{C.M} < -0.80$. The result of the Breit–Wigner fit for the excess depends on the ω scattering angle: its peak and width are $2.25 \pm 0.04\,\mathrm{GeV}$ and 0.25–0.55 GeV, respectively. The possible candidates with high angular momentum are the $G_{17}(2190)$, $H_{19}(2220)$, and $G_{19}(2250)$, all of which have 4-star states [1]. Since all of these candidates have high angular momentum, the angular distributions of these resonance decays could change rapidly at backward angles. This could account for the excess, which becomes smaller at the most backward scattering angle bin. The coupling of the $G_{17}(2190)$ to $p\omega$ decay is supported by the PWA of $\gamma p \to p\omega$ at CLAS [1,16]. The difference between the present data and the theoretical curve can be interpreted as the influence of the $G_{17}(2190)$. However, this interpretation still does not explain the dip structure at $2 \leq \sqrt{s} \leq 2.1\,\mathrm{GeV}$ and $-1.00 < \cos\Theta^{\omega}_{C.M} < -0.95$. The interpretation of the present results may require more than just the contribution of the $G_{17}(2190)$. It is useful for the identification of nucleon resonances with high angler momentum to include very backward angles in the PWA. It is worth mentioning that the very steep s dependence of $\omega\, d\sigma/du$ at $u \sim -0.15\,\mathrm{GeV}^2$, seen in the Daresbury data, is not observed in the LEPS energy range [17].

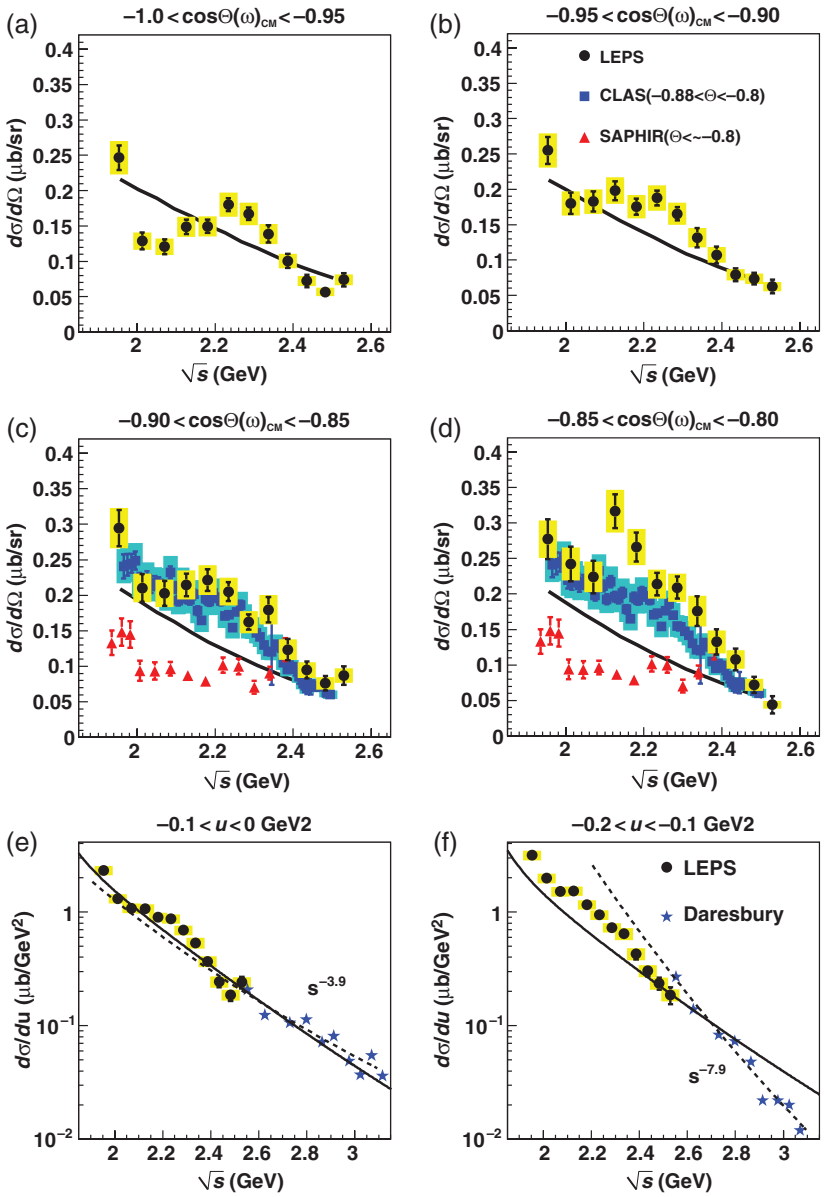

Fig. 3. Differential cross sections for ω photoproduction as a function of $\sqrt{s}$. The black circles are the present results. Shaded bars represent systematic uncertainty. The red triangles, blue squares, and blue stars are the experimental results from SAPHIR, CLAS, and Daresbury, respectively [4,15,17]. Smooth lines represent theoretical calculation and dashed lines represent the result of a power law fit for the Daresbury results [19].

The photon beam asymmetry (Σ) is also sensitive to nucleon resonances. Σ has been measured as $P_\gamma \Sigma \cos 2\phi = (N_v - N_h)/(N_v + N_h)$, where N_v and N_h are the ω yields with the vertically and horizontally polarized photons, respectively [18]. P_γ is the polarization degree of the photon beam, and ϕ is the proton azimuthal angle. The scattering angle of ω is $-1.00 < \cos\Theta^{\omega}_{C.M} < -0.80$ in this measurement. The ω selection cut (Fig. 2(b)) and a missing mass cut of $0.75 < MM(p) < 0.81\,\mathrm{GeV}/c^2$ were used for the ω selection. The amount of background was evaluated in the same way as the analysis of the cross section. The Σ of the background was estimated from the interpolation between Σ of the neighboring mass region of the ω signal. Systematic uncertainty due to the background contribution includes the uncertainty in the Σ of the background and the uncertainty of S/N ratios.

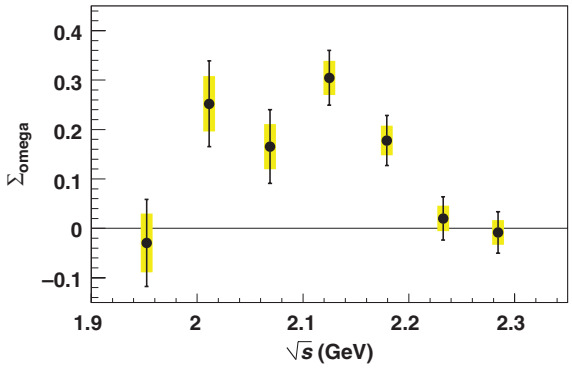

Fig. 4. The photon beam asymmetry of ω as a function of $\sqrt{s}$.

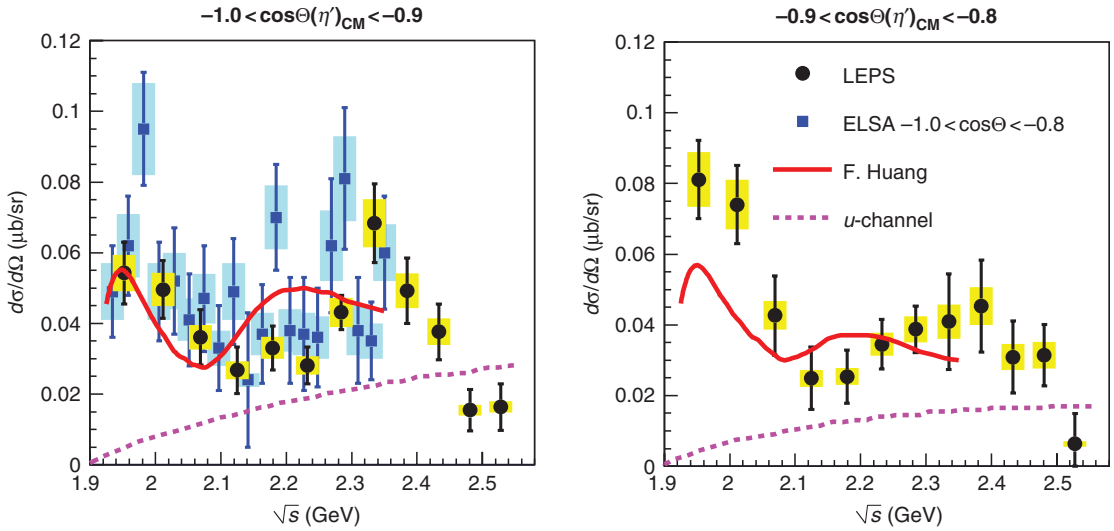

Fig. 5. Differential cross sections for η' photoproduction as a function of $\sqrt{s}$. Shaded bars represent systematic uncertainty. The black circles are the present results. The blue squares are the CB-ELSA results [7]. Smooth lines represent the theoretical calculation by F. Huang in Ref. [21]. Dotted lines represent the u-channel contribution in Ref. [21].

The systematic uncertainty in the measurement of laser polarization is $\delta\Sigma = 0.02$. Figure 4 shows the measured Σ of ω production as a function of $\sqrt{s}$. Σ becomes large at $2 < \sqrt{s} < 2.2$ GeV and vanishes rapidly at $\sqrt{s} > 2.23$ GeV. This result also suggests that there is an influence of nucleon resonances on ω photoproduction at $\sqrt{s} \sim 2.1$ GeV. The region with the large Σ is different from the peak position of the $d\sigma/d\Omega$. It is expected that PWA analysis including the Σ measurement may clarify the resonances involved in ω photoproduction.

Figure 5 shows the differential cross sections for η' production as a function of $\sqrt{s}$. Each panel shows the result at the η' scattering angle regions. The results of CB-ELSA in $-1.0 < \cos\Theta^{\eta'}_{C.M} < -0.8$ are also shown in Fig. 5 [7]. The results of CB-ELSA are consistent with the present result. The uncertainty of $d\sigma/d\Omega$ is reduced substantially and a bump structure at $\sqrt{s} \sim 2.35$ is revealed in the present results. The bump structure at $\sqrt{s} \sim 2.35$ GeV appears clearer in the most backward scattering angle bin, $-1.0 < \cos\Theta^{\eta'}_{C.M} < -0.90$. A small bump at 2.25 GeV found in the previous LEPS result can be seen by slightly changing the energy binning in $-0.9 < \cos\Theta^{\eta'}_{C.M} < -0.80$,

though there is a discrepancy between the present and the previous LEPS results [10]. The confirmation of the small bump at 2.25 GeV requires much higher statistics than the present data. The theoretical calculation is also shown in Fig. 5. This calculation is based on an effective Lagrangian approach, considering the resonances of S_{11}, P_{11}, and P_{13} [21]. Various parameters, such as the resonance mass and width, in this calculation are tuned to reproduce the various experimental results of the $\gamma N \to \eta' N$, $NN \to NN\eta'$, and $\pi N \to \eta' N$ reactions. The dotted lines in Fig. 5 show the u-channel contribution in the theoretical calculation in Ref. [21]. It should be mentioned that the theoretical u-channel contribution at $\sqrt{s} > 2.35$ GeV is just an extrapolation. The $NN\eta'$ coupling constant $g_{NN\eta'}$ in this calculation was assumed to be 1.0. If we compare the present result with the u-channel contribution at $\sqrt{s} > 2.4$ GeV, $g_{NN\eta'} = 1$ seems to be a reasonable assumption. The dominant contribution at backward angles is from nucleon resonances at $\sqrt{s} < 2.10$ GeV and the $\sqrt{s} \sim 2.35$ GeV region, according to the comparison between the LEPS result and the u-channel contribution. Currently, the list of resonances involving η' production strongly depends on models [20,21]. Since the rapid change at only backward angles may indicate resonance with high angular momentum, PWA including the present result will provide important information to reduce the model dependence.

5. Summary

In summary, the ω and η' photoproduction from protons at backward angles has been measured at $E_\gamma = 1.5$–3.0 GeV at the SPring-8/LEPS facility. The ω and η' mesons were identified by detecting forward-scattered protons in the spectrometer and detecting pions from meson decay in the time projection chamber surrounding the target. The differential cross sections for ω mesons are larger than the expected u-channel contribution in the range $2.0 \leq \sqrt{s} \leq 2.4$ GeV. Although a contribution from the $G_{17}(2190)$ resonance is a possible explanation for this excess in the ω differential cross sections, a partial wave analysis including the present data is important to identify the possible resonances. A bump structure in the $\sqrt{s}$ dependence of the differential cross sections for η' mesons was observed at $\sqrt{s} \sim 2.35$ GeV. PWA including the present result will also be useful to reveal the resonances involving η' production.

Acknowledgements

We thank the staff at SPring-8 for providing excellent experimental conditions. We thank A. Sibirtsev and H. Kamano for fruitful discussions. This work was supported in part by the Ministry of Education, Science, Sports and Culture of Japan; the National Science Council of the Republic of China (Taiwan); the National Science Foundation (USA); and the National Research Foundation (Korea).

References

[1] Particle Data Group, Phys. Rev. D **86**, 10001 (2012).
[2] S. Capstick and N. Isgur, Phys. Rev. D **34**, 2809 (1986).
[3] J. Bulava et al., Phys. Rev. D **82**, 14507 (2010).
[4] M. Williams et al., Phys. Rev. C **80**, 65208 (2009).
[5] J. Ajaka et al., Phys. Rev. Lett. **96**, 132003 (2006).
[6] E. F. McNicoll et al., Phys. Rev. C **82**, 35208 (2010).
[7] V. Crede et al., Phys. Rev. C **80**, 55202 (2009).
[8] M. Williams et al., Phys. Rev. C **80**, 45213 (2009).
[9] O. Bartalini et al., Eur. Phys. J. A **33**, 169 (2007).
[10] M. Sumihama et al., Phys. Rev. C **80**, 52201 (2009).
[11] T. Nakano et al., Nucl. Phys. A **684**, 71 (2001).
[12] M. Niiyama et al., Phys. Rev. C **78**, 35202 (2008).

[13] N. Muramatsu et al., [arXiv:1201.4094] [Search INSPIRE].
[14] R. Brun et al., GEANT3.21, CERN-W5013, 1994.
[15] J. Barth et al., Eur. Phys. J. A **18**, 117 (2003).
[16] M. Williams et al., Phys. Rev. C **80**, 65209 (2009).
[17] R. W. Clifft et al., Phys. Lett. B **72**, 144 (1977).
[18] M. Sumihama et al., Phys. Rev. C **73**, 35214 (2006).
[19] A. Sibirtsev, K. Tsushima, and S. Krewald, [arXiv:0202083 [nucl-th]] [Search INSPIRE].
[20] W.-T. Chiang et al., Phys. Rev. C **68**, 45202 (2003).
[21] F. Huang, H. Haberzettl, and K. Nakayama, Phys. Rev. C **87**, 54004 (2013).